4-1-2021

Carbon dots for specific "off-on" sensing of Co^{2+} and EDTA for in vivo bioimaging

Xiangping Wen
Shanxi University

Guangming Wen
Jinzhong University

Wenyan Li
Shanxi University

Zhonghua Zhao
Shanxi University

Xine Duan
Shanxi University

See next page for additional authors

Carbon Dots for Specific "Off-On" Sensing of Co^{2+} and EDTA for *in vivo* Bioimaging

Xiangping Wen[a], Guangming Wen[d], Wenyan Li[b], Zhonghua Zhao[c], Xine Duan[b*], Wenjun Yan[e], John F. Trant[f*], Yingqi Li[b,a*]

[a] Key Laboratory of Chemical Biology and Molecular Engineering of Ministry of Education, Institute of Molecular Science, Shanxi University, Taiyuan 030006, P. R. China

[b] Department of Chemistry, College of Chemistry and Chemical Engineering, Shanxi University, Taiyuan 030006, P. R. China

[c] Institute of Biomedical Science, Shanxi University, Taiyuan 030006, PR China

[d] College of Chemistry and Chemical Engineering, Jinzhong University, Jinzhong 030619, P. R. China

[e] Analytical Instrumentation Center, Institute of Coal Chemistry, Chinese Academy of Sciences, Taiyuan 030001, P. R. China

[f] Department of Chemistry and Biochemistry, University of Windsor, 401 Sunset Avenue, Windsor ON, Canada

*E-mail: duanxe@sxu.edu.cn; j.trant@uwindsor.ca; wkyqli@sxu.edu.cn

Tel: +86 13934562602

Abstract: Fluorescent carbon dots (CDs) were hydrothermally synthesized from a mixture of frozen tofu, ethylenediamine and phosphoric acid in an efficient 64% yield. The resulting CDs exhibit good water solubility, low cytotoxicity, high stability, and excellent biocompatibility. The CDs selectively and sensitively detect Co^{2+} through fluorescent quenching with a detection limit of 58 nM. Fluorescence can be restored through the introduction of EDTA, and this phenomenon can be used to quantify EDTA in solution with a detection limit of 98 nM. As both analytes are detected by the same CD platform, this is an "off-on" fluorescence sensor for Co^{2+} and EDTA. The technique's robustness for real-world samples was illustrated by quantifying cobalt in tap water and EDTA in contact lens solution. The CDs were also evaluated for *in vivo* imaging as they show low cytotoxicity and excellent cellular uptake. In a zebrafish model, the CDs are rapidly adsorbed from the intestine into the liver, and are essentially cleared from the body in 24 hours with no appreciable bioaccumulation. Their simple and efficient synthesis, combined with excellent physical and chemical performance, renders these CDs attractive candidates for theranostic applications in targeted "smart" drug delivery and bioimaging.

Keywords: Carbon Dots, Co^{2+}, EDTA, bioimaging, metabolism, zebrafish

1. Introduction

Carbon quantum dots (CDs), carbon nanoparticles under 10 nm in diameter, are simple to synthesize, and exhibit excellent optical sensitivity and stability along with low cytotoxicity and excellent physiological clearance [1-4]. Surface modification can tune the solubility and recognition or targeting ability of the CDs [5, 6]. They are suitable fluorescent probes for ion sensing, catalysis, optoelectronic devices, anti-counterfeiting, bio-imaging, and drug delivery applications [7-12]. For instance, CDs have been used as potential drug candidates to design blood-brain barrier permeable nanomaterials and apply them to the treatment of Alzheimer's disease. CDs can penetrate the zebrafish blood-brain barrier and distribute to the brain where they have a high propensity for localizing to the zebrafish forebrain [13]. For many of these applications they are superior to complex synthetic organic fluorescent probes. They are particularly promising for applications that rely on ion-sensing as they can experience electron transfer, by chelation between pacifying CD-surface functional groups and the ion analyte; this can increase, decrease, or chromatically shift the fluorescence intensity of the CDs [14]. Sensitivity and selectivity are dependent on the affinity between the active groups on the surface of the CDs and the target metal ion [15, 16]; one useful approach to generate this specificity for certain metal ions is to dope with heteroatoms to introduce reactive functionalities [17, 18]. This affinity for specific ions means that CDs can be coupled with potent ion chelators to generate “off-on” fluorescent sensors.

Cobalt (Co) is a physiologically essential mineral, albeit needed in very low quantities, primarily as a component in vitamin B12 which is essential for DNA biosynthesis; deficiency is especially dangerous for inhibiting erythropoiesis and myelin synthesis [19]. However, excessive intake of Co can cause asthma, cramps, diarrhea, rhinitis, hypotension, bone defects, stomach disorders, vasodilation and cancer [20, 21]. The maximum concentration of Co^{2+} in irrigation watering and livestock watering is limited to 0.05 and 1.0 $mg \cdot L^{-1}$, respectively (Environmental Bureau of Investigation, Canadian Water Quality Guidelines) [19].

Ethylenediaminetetraacetic acid (EDTA) is an excellent metal chelator commonly used in detergents, liquid soaps, cosmetics, and anticoagulants. Emergency use of EDTA for lead, or other heavy metal poisoning [22, 23]; however, the rise of so called chelation therapy for non-acute cases can lead to misuse [24]. EDTA has been reported to induce allergic dermatitis in humans [25, 26], and can also cause hypoglycemia and hypocalcemia in the blood [27].

Quantifying Co^{2+} and EDTA levels has been accomplished with CDs previously [28-30]. For example, Bano and colleagues prepared nitrogen-rich CDs for Co (II) detection [31]. Wu and colleagues published nitrogen-doped CDs for the determination of Co^{2+} in aqueous media [32]. Narola et al. used reverse phase HPLC method to detect EDTA in drugs [33]. Krokidis et al. used ion chromatography to determine EDTA in pharmaceutical preparations and canned food [34]. But these detection techniques often involve cumbersome sample preparation, expensive equipment or unsatisfactory detection limits [35-38]. Recently, fluorescent nanomaterials, such as organic nanoparticles and semiconducting quantum dots, have been widely used in the field of sensing [39, 40]. However, the high cytotoxicity and low biocompatibility of these materials have limited their practical application. Therefore, there is an urgent need to find a new type of green material to quickly and sensitively detect both Co^{2+} and EDTA.

At present, a CDs-based fluorescence sensing method has not been established to simultaneously detect Co^{2+} and EDTA. Moreover, there are few reports on the bioeffects of CDs *in vivo* [41]. Additional studies on the *in vivo* uptake, metabolism, and toxicity of CDs are still needed. As zebrafish and human genes are highly similar, this very small, easy to handle and maintain fish, is an excellent model organism [42, 43].

Herein, we developed a facile and inexpensive strategy for the fabrication of nitrogen and phosphorus co-doped fluorescent CDs in high yield. The hydrothermal treatment of a mixture of frozen tofu, ethylenediamine and phosphoric acid provided the CDs we use for various applications in fluorescence imaging both *in vitro* and *in vivo* (**Fig. 1**).

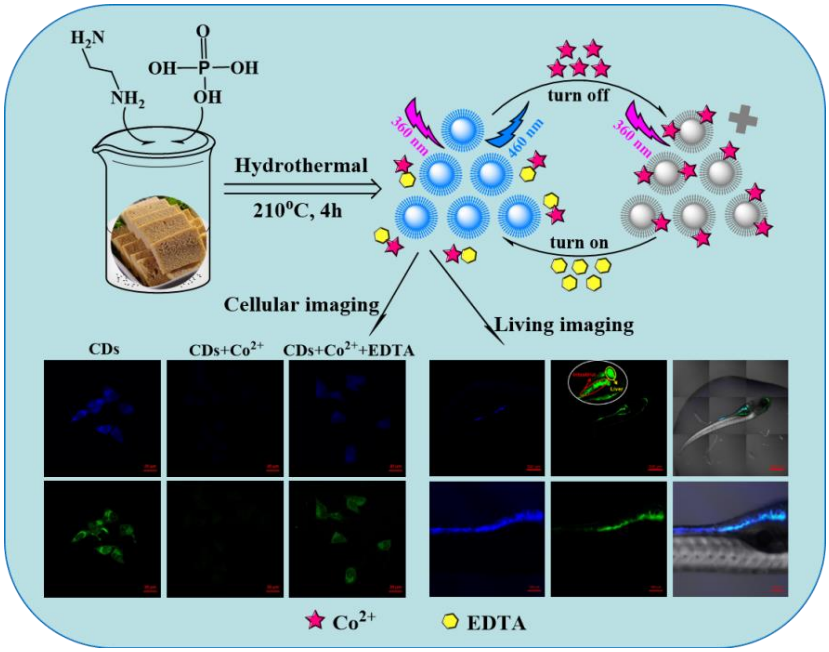

Fig. 1 Graphical representation of the formation, sensing mechanism, cellular imaging application and *in vivo* fluorescence of the CDs

2. Materials and methods

2.1. Materials

Frozen northern tofu was bought from a *Meet all* supermarket (Taiyuan, China). Phosphoric acid and ethylene diamine (Tianjin Dengfeng Chemical Co., Ltd); disodium hydrogen phosphate and sodium dihydrogen phosphate (Tianjin Sailboat Chemical Reagent Technology Co., Ltd); quinine sulfate and methyl-β-cyclodextrin (M-β-CD) (Shanghai Aladdin Biochemical Technology Co., Ltd.); MTT reagent and streptomycin (Beijing Soleil Technology Co., Ltd.); DMEM (Shanghai Beinuo Biotechnology Co., Ltd.); FBS (Sijiqing brand, Hangzhou, China); trypsin (Shanxi Biotech Biotechnology Co., Ltd); sucrose (Shanghai Aibi Chemical Reagent Co., Ltd.); and sodium azide (Chengdu Kelon Chemical Reagent Factory) were used as received without further purification. The HeLa cells were provided by the Genetic Engineering Center of Shanxi University. 0.1 M of various metal anions and cations (Cr^{3+}, Pb^{2+}, Ca^{2+}, Fe^{3+}, Bi^{3+}, K^{+}, Na^{+}, Cu^{2+}, Ba^{2+}, Mn^{2+}, Hg^{2+}, Mg^{2+}, Cd^{2+}, Zn^{2+}, Al^{3+}, Ni^{2+}, Co^{2+}, S^{2-}, I^{-}, Br^{-}, NO_3^{-}, CO_3^{2-}, SO_4^{2-}, CN^{-}, SCN^{-}, $C_2O_4^{2-}$, CH_3COO^{-}, NO_2^{-}, SO_3^{2-}, $S_2O_3^{2-}$, PO_4^{3-}, ClO_4^{-}, BrO_3^{-}, CrO_4^{2-}) were prepared using their chloride, or

sodium salts. Aqueous solutions of 0.01 M of EDTA, Cysteine (Cys), Glutathione (GSH), Homocysteine (Hcy), Tyrosine (Tyr), Lysine (Lys), Arginine (Arg), Phenylalanine (Phe), and Ascorbic Acid (AA) were prepared from dry agents

2.2. Synthesis of CDs

The frozen tofu was cut into 5 mm square pieces with a scalpel which were then washed extensively with distilled water, and then dried in an oven at 50 °C for later use. To create the CDs, 0.5 g of the above dried tofu cubes was placed in a beaker; we then added 4 mL of phosphoric acid and 5 mL of ethylenediamine sequentially with continuous stirring. 0.5 g of the reaction mixture was placed into a hydrothermal reactor (50 mL, Shanghai Kexing Instruments), and 20 mL of deionized water was added. The mixture was thoroughly mixed, and then placed in a 210 °C oven for 4 hours. The reactor was then allowed to cool naturally to ambient temperature, removed from the reactor, and centrifuged for 8 minutes at 8000 RPM to sediment any residual solids, and the supernatant decanted and collected. This was then dialysed against distilled water (MWCO = 500-1000 Da) with two changes of liquid for a total of 24 hours to obtain isolated CDs. This solution was lyophilized to provide 320 mg of the CDs as a pale yellow powder.

2.3. Characterization

The particle size and zeta potential were determined using a Malvern Zetasizer Nano ZS90. Transmission electron microscopy (TEM) images were acquired by a JEM-2100 instrument with an acceleration voltage of 200 kV (JEOL, Japan). Fluorescence spectra were obtained on a fluorescence spectrometer (model F-280, Gangdong Technology, Tianjin). Ultraviolet absorption spectra were acquired using a Cary 50 Bio UV-Vis spectrometer (Agilent, USA). The infrared spectrum was obtained on an FTIR-8400S (Shimadzu, Japan) spectrometer. Raman spectra were collected on a Bruker Senterra dispersive Raman microscope. X-ray photoelectron spectroscopy (XPS) was conducted using an AXIS ULTRA DLD electronic spectrometer (Japan). The fluorescence lifetime was measured on an Edinburgh FLS920 spectrometer (UK). The relative fluorescence quantum yield (QY) of the CDs

was calculated using the formula $\Phi_x=\Phi_{std}\ I_x\ A_{std}\ \eta^2_x / (I_{std}\ A_x\ \eta^2_{std})$. Where I_x and I_{std} represent the fluorescence intensity of the CDs and reference, respectively; A_x and A_{std} represent the optical densities of the CDs and the reference, respectively; and η_x and η_{std} represent the refractive indices of the CDs and the reference, respectively. The standard used was quinine sulfate, with a QY of 0.54 in a 0.1 M H_2SO_4 at 360 nm excitation. Cellular imaging was conducted using a laser scanning confocal microscope (LSCM; Leica TCSSP5, Germany) and a fluorescence microscope (ZEISS, Vert. A1, Germany).

2.4. Detection of Co^{2+} and EDTA.

To conduct the sensitivity tests, aliquots of 200 μL of an aqueous solution of CDs (1 mg/mL) was added to 600 μL of a pH 5.0 Tris-HCl solution to measure the original fluorescence intensity. To the different aliquots of this solution, 2 μL of various chlorides with a concentration of 0.1 M (Mg^{2+}, Pb^{2+}, Hg^{2+}, K^+, Cd^{2+}, Cr^{3+}, Bi^{3+}, Zn^{2+}, Na^+, Al^{3+}, Ca^{2+}, Fe^{3+}, Mn^{2+}, Ba^{2+}, Cu^{2+}, Co^{2+}, Ni^{2+}), or 0.1 M of various sodium salts (NO_3^-, CO_3^{2-}, SO_4^{2-}, $C_2O_4^{2-}$, CH_3COO^-, NO_2^-, SO_3^{2-}, $S_2O_3^{2-}$, PO_4^{3-}, ClO_4^-, BrO_3^-, CrO_4^{2-}) were added with mixing. Noting the high selectivity for cobalt (II), the same volume of $CoCl_2$ solutions of different concentrations were added to generate a concentration scan. All excitation occurred at 360 nm. In all cases, fluorescence intensity was recorded 60 seconds after addition with a slit width of 5 nm. Finally, we studied the fluorescence recovery effects of different anions and small molecules (S^{2-}, I^-, Br^-, NO_3^-, CO_3^{2-}, SO_4^{2-}, CN^-, SCN^-, AA, GSH, Hcy, Arg, Tyr, Lys, Phe, Cys, EDTA) on the CDs-Co^{2+} system. Solutions (0.05 M) of these anions (as their sodium salts) and small molecules (15 μL) were added to a solution of the CDs-Co^{2+} system (800 μL) generated from the above protocol. The solution was thoroughly mixed, and the fluorescence intensity was measured. With EDTA showing significant activity, an EDTA concentration scan was performed under the same protocol using different stock solutions of EDTA to vary the final concentration. The $(F_0-F)/F_0$ ratio was used to represent the recovery efficiency of EDTA on the CDs-Co^{2+} system, where F_0 and

F are the measured fluorescence emission at 460 nm when excited with 360 nm light in the absence and presence of EDTA respectively.

2.5. Analysis in complex matrices

To demonstrate the feasibility of the sensor in an actual sample, tap water (10 mL, Taiyuan municipal water, China) was centrifuged at 8,000 rpm for 10 minutes to remove macroscopic particulate matter, followed by filtration through a 0.45 μm pore size filter membrane. The analysis solution was prepared by diluting 200 μL of CDs (1 mg/mL) with 600 μL of a pH 5.0 Tris-HCl solution. The fluorescence intensity of this, F_0 was obtained. Then, the tap water sample, spiked with Co^{2+} standard solutions, was added to the analysis solution (final concentrations: 0.3, 0.4, and 0.5 μM of Co^{2+}), and the fluorescence intensity (F) was measured. The Co^{2+} concentration was calculated according to the linear equation. Next, we added a contact lens care solution containing a standard EDTA concentration (0.05 mg/mL) to the above-mentioned Co^{2+} quenched CDs tap water system (final concentrations: 0.4, 0.7, and 0.9 μM of EDTA), measured the fluorescence intensity, and calculated the concentration of EDTA according to our linear equation.

2.6. Fluorescence imaging

HeLa cells (density of 1.0×10^5 cells) were incubated in a 35 mm culture dish overnight at 37.5 ºC in BMEM media. The spent media was removed, and the cells were incubated with 400 μg/mL of CDs in BMEM media for 2 h. To this solution we added 1 ml of pH 7.4 PBS to the cell culture dish, and gently shook to wash, removing any unabsorbed CDs. The supernatant was aspirated away, and replaced with a fresh 1 mL of PBS; the process was repeated for a total of three washes, before 1 ml of PBS was added, and the cells imaged under LSCM. Next, 3.5 μL of a 0.1 M Co^{2+} in PBS was added to the living cell system and incubated for 5 minutes. Images were obtained. Subsequently, 25 μL of EDTA with a concentration of 0.05 M was added to the cell plate. Again, fluorescence images of the cells were obtained by LSCM.

2.7. In vivo imaging and toxicity

Zebrafish were induced to lay eggs under light stimulation; the embryos were then harvested and washed and incubated with standard E3 medium (5 mM NaCl, 0.17 mM KCl, 0.33 mM $CaCl_2 \cdot 2H_2O$, 0.33 mM $MgSO_4 \cdot 7H_2O$). The zebrafish larvae, 5 dpf, were transferred to a 6-well plate (20 larvae per well), and incubated with E3 medium (5 mL) containing 3 mg/mL of CDs. After 24 hours, representative zebrafish were fixed and photographed using a laser confocal microscope. The remaining zebrafish were transferred to E3 medium without CDs and were maintained until death with medium changes every day. The fluorescence of the intestinal tract and liver over the time course was monitored by laser confocal microscopy to evaluate the metabolism of CDs in the body. In a second study, 5 ml of E3 medium containing different CD concentrations (0, 0.5, 1, 3, 5, 7 mg/mL) were evaluated in a six-well plate with 20 Zebrafish added to each well. The survival of the fish was observed and recorded over time to calculate the in vivo toxicity of the carbon dots to the zebrafish.

2.8. Information encryption/decryption

We filled a pen (Morning light, Gel refill) with an aqueous solution of CDs and drew various patterns on filter paper (beimu). These were naturally air-dried and then placed under a 365 nm UV light. We then sprayed an aerosolized 0.1 M Co^{2+} solution onto the filter paper and placed it under the UV light again. Finally, a similarly formulated EDTA solution (0.1 M) was sprayed onto the filter paper and photographed under the same UV light.

3. Results and discussion

3.1. The synthesis and characterization of CDs

The nitrogen and phosphorus co-doped CDs were successfully prepared in a one-step hydrothermal reaction of frozen tofu, ethylenediamine and phosphoric acid (**Fig. 1**). Protein-rich tofu provides a rich source of carbon and nitrogen for the synthesis of CDs, while ethylenediamine and phosphoric acid contribute to the formation of surface functional groups on the CDs. The resulting CDs have good

dispersibility, are highly soluble in water, and are obtained in a high yield of 64% based on the mass of the tofu starting material. The fluorescence intensity of CDs prepared without the addition of ethylenediamine and phosphoric acid, or with only either one of ethylenediamine or phosphoric acid is relatively weak (**Fig. S1a-c**). However, with both additives, the fluorescence intensity of the prepared CDs significantly increased. A scan of the relative ratios of the additives was conducted and identified that a 4:5 (v/v) ratio of phosphoric acid to ethylenediamine provided the greatest degree of fluorescence for the resulting nanoparticles (**Fig. S1d**).

Transmission electron microscopy (TEM) images (**Fig. 2a**) shows that the CDs are well dispersed and have a diameter in the range of 2-4 nm, with an average particle size of 2.9 nm. The corresponding Scanning probe microscope (SPM) image (**Fig. 2b**) revealed a typical topographic height of 2.5-3.5 nm (**Fig. 2c**), which supports the proposed spherical geometry of the CDs**.** The DLS indicates a mean hydrodynamic size of 8.1±0.60 nm (**Fig. S2**), which, as expected, is larger than the result of TEM, with the difference resulting from the solvation sphere around the nanoparticle.

Fluorescence spectroscopy and UV-vis absorption are effective tools for characterizing the optical properties of CDs. The two most distinct absorption peaks in the CD UV-vis spectrum are at 282 nm and 323 nm (**Fig. 2d**). That at 282 nm is due to the π-π* transition of the C=C bonds in the sp^2 domain. The peak at 323 nm is due to the n-π* transition of conjugated C=O bonds [44]. The optimal excitation (λ_{ex}) and emission (λ_{em}) wavelengths for the CDs to maximize the amplitude of emission are at 360 and 460 nm, respectively (**Fig. 2d**). Aqueous solutions of CD illuminated with 365 nm UV light emit strong blue fluorescence (inset), while the CD solid powder is bright yellow. As expected, fluorescence is highly dependent on the wavelength of excitation (**Fig. 2e**) [45]. As the excitation wavelength increases, the emission red-shifts and fluorescence intensity decreases. This excitation-dependent photoluminescence (PL) is important for multicolor bioimaging, especially *in*

vivo. Using quinine sulfate as a reference, the fluorescence quantum yield of these CDs was measured to be 9.5% (in **Fig. S3** and **Table S1**), which is higher than that of other previously reported N, P co-doped CDs [46-48]. The XRD pattern of the CDs (**Fig. S4**) showed a broad peak centered at 2θ=23.18, consistent with an amorphous carbon phase, which arises due to the disruption introduced into the lattice by N-, and P-containing groups [49].

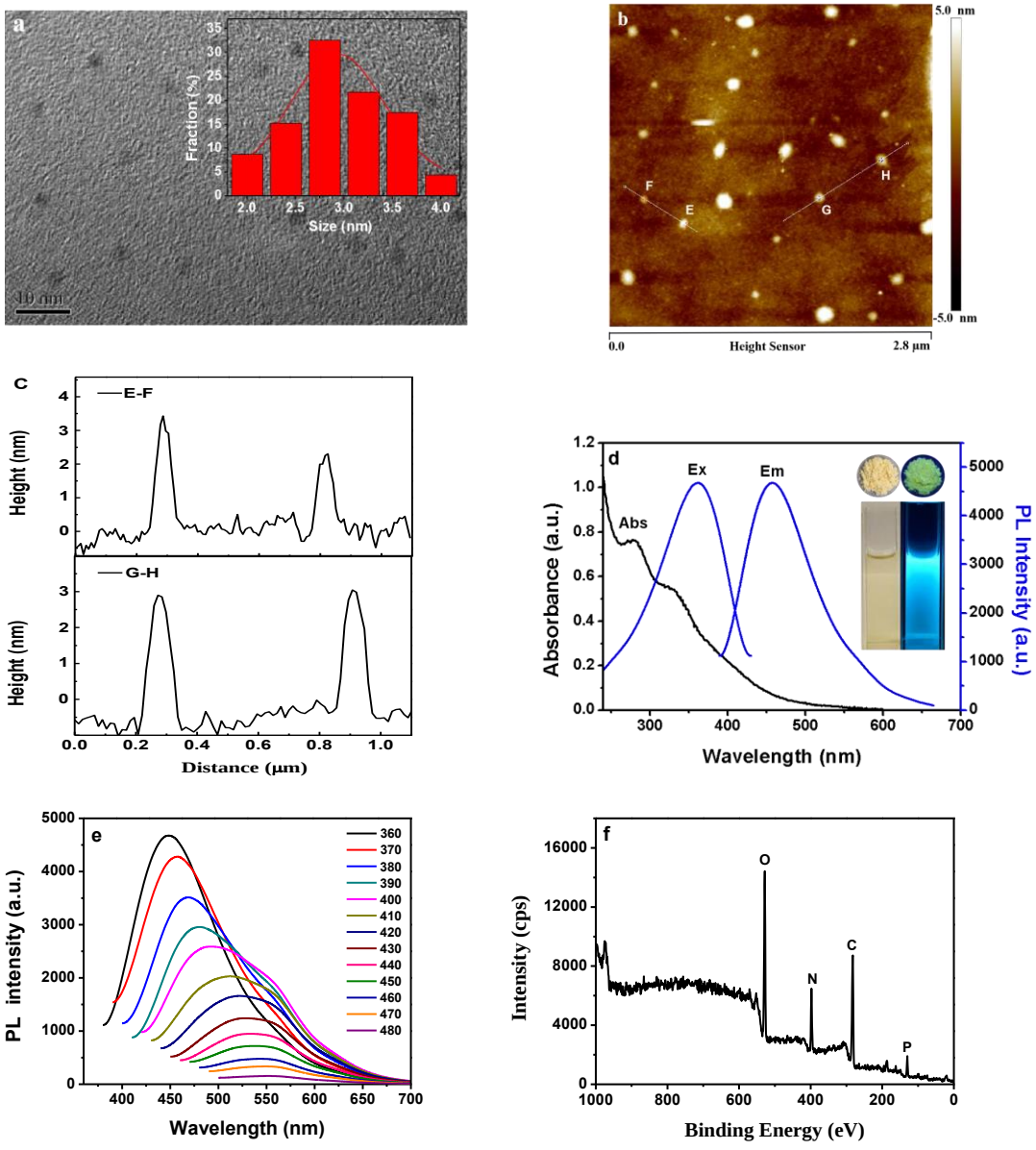

Fig. 2 Characterization of the CDs. (a) A representative TEM image of the CDs. (Inset: size distribution histogram) (b) SPM image of the CDs on a Si substrate. (c) Height profile along the lines in (b). (d) The absorbance, excitation and emission spectra of the CDs. The insets are photographs of both powder and aqueous solutions of CDs under daylight (left) and 365 nm UV

light (right), respectively. (e) The fluorescence emission spectra of the CDs under different excitation wavelengths. (f) The XPS spectrum of the CDs.

The Raman spectrum shows two peaks at 1379 cm^{-1} (D band) and 1585 cm^{-1} (G band; **Fig. S5a**), attributable to the disordered surfaces and the sp^2 carbon networks respectively [50]. The intensity ratio of D and G bands (I_D/I_G) is 0.87, revealing an amorphous carbon phase of CDs [51].

The composition and identity of present functional groups was also examined by Fourier transform infrared spectroscopy (FTIR) and X-ray photoelectron spectroscopy (XPS). The FTIR spectrum (**Fig. S5b**) shows that the CD surface is dotted with N-H (3473 cm^{-1}), O-H (3228 cm^{-1}), -CH_2 (3007 cm^{-1}), C=O (1631 cm^{-1}), C=C (1571 cm^{-1}), C-N (1504 cm^{-1}), C-O (1402 cm^{-1}), P=O (1076 cm^{-1}), and P-O (870 cm^{-1}) functionalities. The XPS spectrum confirms that the CDs are mainly composed of C, N, O and P in a ratio of 55.4: 14.1: 25.7: 4.8 (**Fig. 2f**, **Table S2**). The four peaks at 284.8, 399.6, 532.2 and 133.3 eV belong to C_{1s}, N_{1s}, O_{1s} and P_{2p}, respectively. The C_{1s} spectrum (**Fig. S5c**), reveals the presence of three different types of carbon, with the signals at 284.9, 286.4 and 288.2 eV corresponding to graphitic or aliphatic carbon (C−C/C=C), C-N and C=O/C=N, respectively. The O_{1s} spectrum (**Fig. S5d**) contains two distinct signals at 530.8 eV for P=O, and 531.9 eV for C-OH/C-O-C. In the N_{1s} spectrum (**Fig. S5e**), the two peaks at 399.7 and 400.5 eV arise from C-N-C and N-H groups. Finally, the P_{2p} spectrum displays two peaks at 132.51 eV (P-O) and 133.21 eV (P-C) (**Fig. S5f**). These results combine to strongly suggest that the P and N are chemically incorporated into the CD matrix.

The zeta potential of the CDs was measured to be -19 mV, which may be caused primarily by exposure of -COO^- groups on the surface. The rich mixture of functional groups not only induce a negative charge on the surface of the CDs, but also increase the materials' hydrophilicity and stability, essential for any cell imaging application.

3.2. Fluorescence sensing of Co^{2+} and EDTA

As the surface of the CDs is negatively charged, they could potentially be used for metal-ion-specific detection. We screened a library of salts against the materials looking for fluorescence quenching as the readout (**Fig. 3a, Fig. S6**). Little effect was observed for any ion except Co^{2+}. When the CDs were prepared without the addition of ethylenediamine and/or phosphoric acid, they showed no fluorescence-response sensitivity to any cation (**Fig. S7**). Closer examination of the Co^{2+} effect demonstrated dose dependence (**Fig. 3b, 3c**) confirming the CD's suitability as a "on-off" fluorescent probe for Co^{2+}. Linearity is good between 0 to 0.5 μM with a limit of detection of 58 nM. Next, we explored the sensing mechanism that was causing the quenching. The absorption spectra of the Co^{2+} and the emission spectra of the CDs overlap (**Fig. S8a**), resulting in the generation of an inner filter effect (IFE) [52]. However, the average fluorescent lifetime of the CDs and CDs-Co^{2+} systems were 5.63 ns and 5.56 ns, respectively (**Fig. S8b**), indicating that the adsorption of Co^{2+} did not change the fluorescence lifetime of the CDs. The results suggest that the static quenching of CDs may be caused by a specific interaction between the CDs and Co^{2+} [53]. In addition, we explored the fluorescence quenching effect as a function of temperature (**Fig. S8c**). When the temperature increases, the slope of the Stern-Volmer plot decreases, further supporting that quenching occurs through a static mechanism [54]. This is consistent with the fact that Co^{2+} readily forms complexes with carboxylates and amines, like the functional groups on the surface of our CDs. Hence cobalt-specific CD quenching is likely due to a combination of the IFE and static quenching that occur upon adsorption.

In order to demonstrate the suitability of the CDs for the detection of Co^{2+} in real samples, the content of Co^{2+} in tap water was evaluated. We spiked municipal tap water with known amounts of Co^{2+} (final concentrations: 0.3, 0.4, and 0.5 μM), and measured fluorescence. Using our method, we calculated the concentrations 0.29, 0.41, and 0.49 μM respectively; the other components of

the tap water did not interfere with the assay (**Table 1**). The CDs are appropriate for quantitative detection of Co^{2+} in the environment.

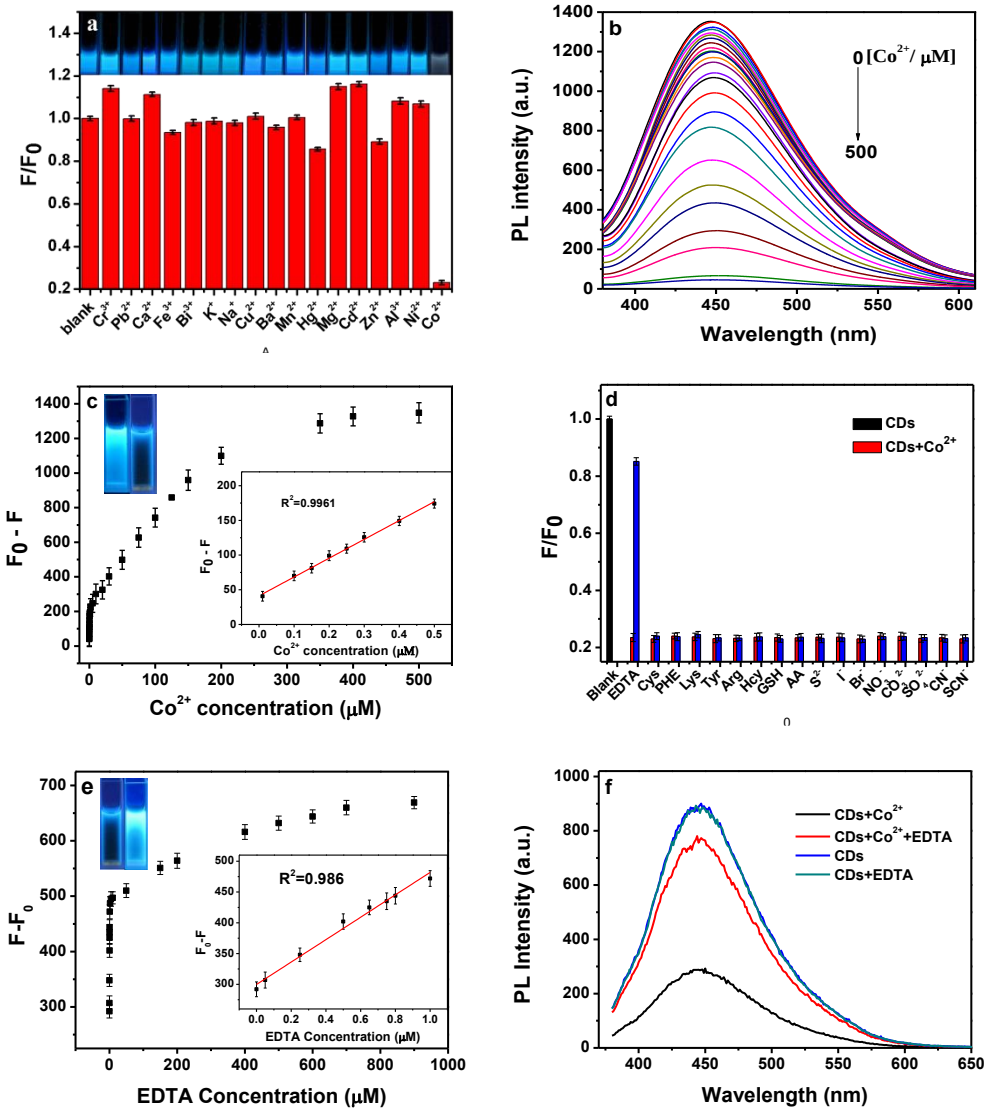

Fig. 3 Fluorescent response of CDs to Co^{2+} and EDTA. (a) Fluorescence intensity ratio (F/F_0) of CD solutions (0.25 mg/mL) in the presence of Co^{2+} (250 μM) and various other common metal ions. Insets show photographs of the CD solution after the addition of 300 μM of the different metal ions under 365 nm UV lamp. (b) Effect of different concentrations of Co^{2+} (from 0 to 500 μM) on the fluorescence emission intensity of CDs. (c) Relationship between F_0-F and the Co^{2+} concentrations. F_0 and F represent the PL intensity of the initial CD solution and the solution after Co^{2+} is added, respectively. Inset: pictures of the CD solutions neat, and in the presence of 300 μM Co^{2+} under UV light (365 nm). (d) Fluorescence intensity ratio (F/F_0) of CD-Co^{2+} system with the

addition of EDTA (920 μM) and various other anions and small molecules. (e) Relationship between F-F_0 and EDTA concentration for CD-Co^{2+}; F_0 and F represent the PL intensity of the CD solution prequenched with 250 μM Co^{2+}, and after EDTA was added at the provided concentrations respectively. Inset: pictures of the CD-Co^{2+} solutions with the addition of no EDTA, and with the addition of 800 μM EDTA under UV light (365 nm). (f) Fluorescence spectra of CDs under different environmental conditions (CDs concentrations: 0.25 mg/mL; Co^{2+} concentrations: 250 μM; EDTA concentrations: 920 μM).

Inspired by the strong affinity between Co^{2+} and EDTA, we speculated that EDTA may restore the fluorescence of a quenched CD-Co^{2+} system. Evaluating it and a variety of other small molecules and anions, it was clear that it does (**Fig. 3d**), and it does in a dose-dependent matter (**Fig. 3e**), restoring 80.6% of the initial intensity before plateauing (**Fig. 3f**). The dose effect is highly linear in the 0-1 μM range with a detection limit of 98 nM. Compared to previously reported methods for EDTA quantification [55, 56], this fluorescence sensing method has the advantages of convenience and simplicity.

Although fluorescence recovery is only 80%, after three cycles it stabilizes at 65% of the original fluorescence and can be recycled repeatedly after that point with negligeable additional loss of activity (**Fig. S9**). In order to demonstrate the suitability of Co^{2+}-quenched CDs for the detection of EDTA in actual samples, the EDTA content in commercial contact lens care solutions was quantified (**Table 1**). Contact lens solution (0.5mg/mL EDTA) was added to the CDs-Co^{2+} tap water system (final EDTA concentrations: 0.4, 0.7, and 0.9 μM), and the determined concentrations were 0.42, 0.72, and 0.89 μM. The CDs are suitable for the detection of EDTA in actual samples.

Table 1. Practical Sample Detection of CDs for Co^{2+} and EDTA

sample no.	1	2	3
Co^{2+} added (μM) to tap water	0.3	0.4	0.5
Co^{2+} detected (μM)	0.289	0.413	0.491

error analysis	±1.81	±2.13	±1.46
RSD (%)	3.03	2.54	1.78
recovery (%)	96.3	103.3	98.2
EDTA in contact lens care solution added (μM)	0.4	0.7	0.9
EDTA detected (μM)	0.417	0.719	0.887
error analysis	±1.91	±2.08	±1.54
RSD (%)	2.64	1.87	2.05
recovery (%)	104.3	102.7	98.6

Our detection limits for Co^{2+} and EDTA were compared with previously published tools (**Table 2**). Our system is among the more sensitive for Cobalt, and is almost as sensitive as an HPLC protocol for EDTA; however a one-off fluorescence measurement is far simpler to conduct than an HPLC method suggesting that our CDs could be more useful. These CDs are among the most sensitive tools to quantitatively detect Co^{2+} and EDTA. However, their mode of action makes them potentially promising for *in vivo* applications.

Table 2. Comparison with some previously reported of detection for Co^{2+} and EDTA

Materials or technique	LOD of Co^{2+} (nM)	LOD of EDTA (μg/mL)	refs.
N-carbon quantum dots	120		Bano et al. (2019) [31]
N-CDs	250		Jing et al. (2019) [32]
CDs	390		Zhao et al. (2019) [35]
N-doped CDs	230.5		Du et al. (2020) [57]
N,S-doped CDs	5		Li et al. (2014) [58]
Cetrimonium bromide-passivated CDs	0.67		Shi et al. (2013) [29]
HPLC		0.023	Hallaj et al. (2014) [36]

Z-CDs		0.12	Yang et al. (2018) [37]
flame atomic absorption spectroscopy		2	Sharratt et al. (2009) [27]
CDs	58	0.033	this work

3.3. Intracellular accumulation and endocytosis of CDs

Stability, low toxicity and biocompatibility are essential for biological applications. First, we studied the optical stability of the CDs to the environment (**Fig. S10a**). The fluorescence is largely independent of pH over a range of 2-12. Similarly, CD fluorescence intensity is independent of ionic strength from 0-1.0 M KCl (**Fig. S10b**). The CDs are resistant to photobleaching, with no change to fluorescence, even after constant UV irradiation (365 nm, 16 W) for four hours (**Fig. S10c**); they also show only very minor loss in fluorescence upon extended (three month) storage in solution (**Fig. S10d**). In addition, pH and temperature basically do not affect the capability of CDs against Co (**Fig. S11**). The CDs have excellent optical stability.

An MTT assay was used to assess *in vitro* cytotoxicity of CDs against HeLa cells over a 24 hour time-course (**Fig. S12**). Even at a very high 600 μg/mL (effective concentration is below 250 μg/mL) cell survival rate was still above 87%. Cell viability was within error of the negative control at 200 μg/mL. The CDs are effectively non-toxic well above their effective concentration.

Due to the low toxicity and excellent fluorescence properties of CDs, we explored the potential of cell imaging. **Fig. S13** shows fluorescent images of HeLa cells incubated with CDs. Multicolor fluorescent images can be acquired by selecting different lasers owing to excitation-dependent emission characteristics of the CDs and demonstrating that they readily localize to the cells. When excited by a light source of 405 and 488 nm, respectively, a multicolor cell imaging pattern in both blue and green fluorescence can be obtained (due to differences in emission maxima depending on excitation wavelength, **Fig. 4**). After adding Co^{2+} to the system (as $CoCl_2$, 350 μM final

concentration), the intracellular fluorescence was largely quenched. However, the fluorescence was restored upon addition of EDTA.

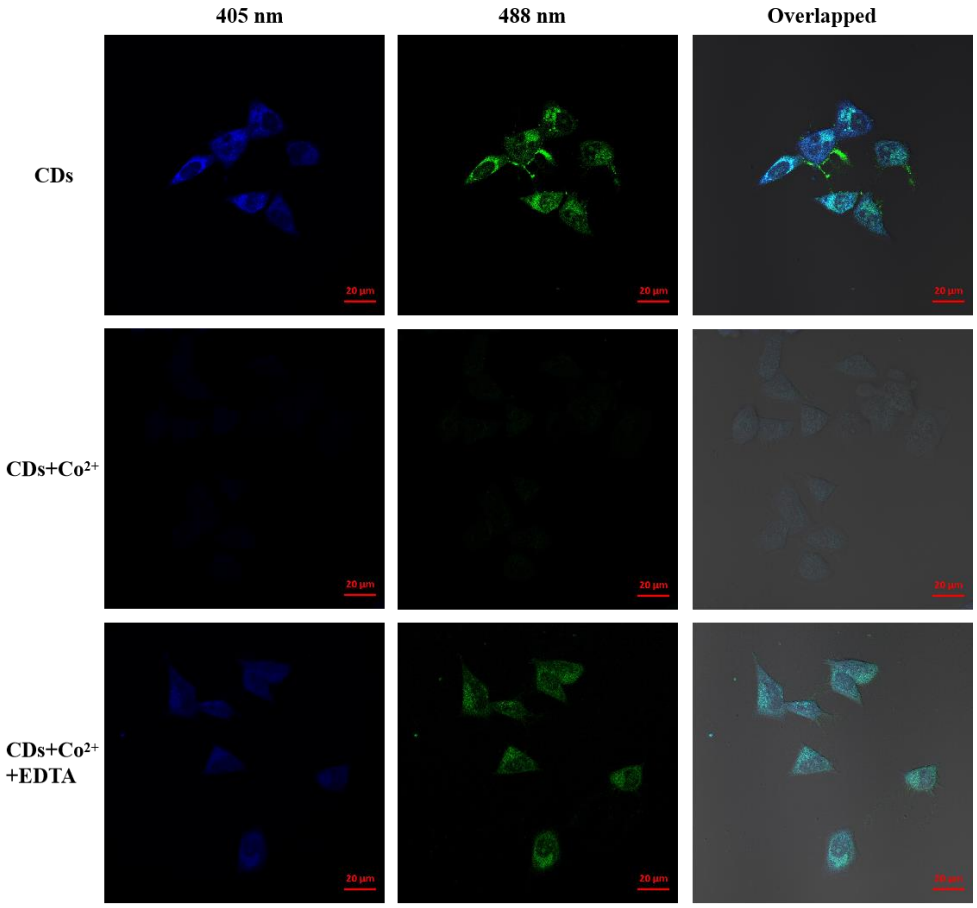

Fig. 4 Cellular imaging of HeLa cells incubated with CDs (400 μg·mL^{-1}), followed by sequential treatment with Co^{2+} and EDTA under both 405 nm and 488 nm excitation.

In order to study the cellular uptake kinetics of the CDs, the fluorescence intensity of CDs in HeLa cells as a function of time was measured by flow cytometry using our previously reported method [59]. In this experiment, the fluorescence intensity gradually increases as the incubation time proceeds (**Fig. S14a**), largely plateauing after 1 h (**Fig. S14b**). A single exponential function fit predicts a rate constant of uptake (k) of about 0.08 min^{-1}, implying that it takes nearly 9 min for cells to absorb 50% of their maximum amount of CDs. **Fig. S14c** displays a quick analysis of the effect of additives on cellular uptake to probe mechanism. This pattern (moderate impact from sodium azide and β-cyclodextrin, with significant inhibition by sucrose or lower temperatures) is consistent with uptake occurring primarily through the clathrin-mediated endocytic pathway [60-62].

3.4. Uptake and metabolism of CDs in zebrafish

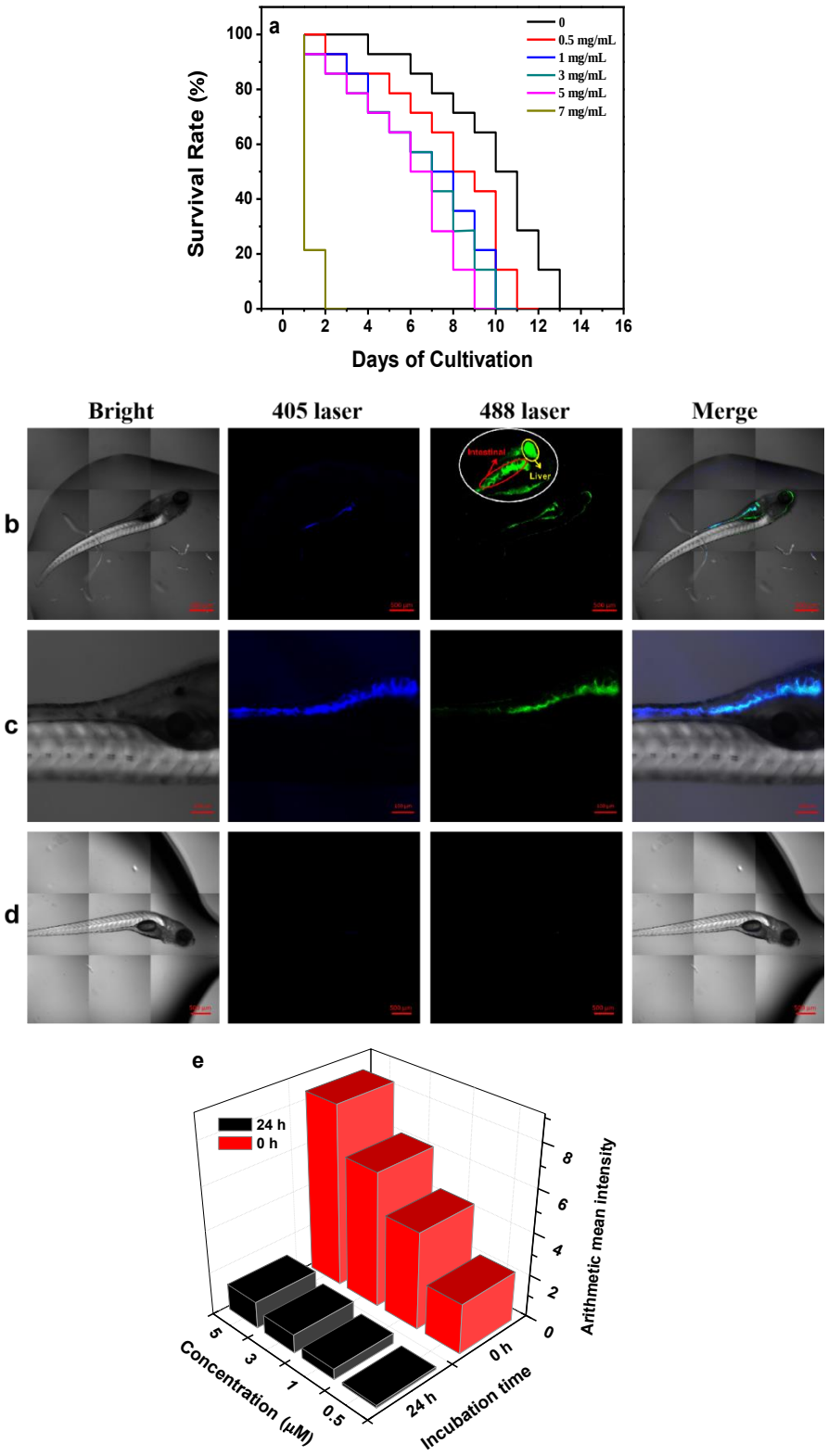

Fig. 5 *In vivo* biological effect of zebrafish. (a) Kaplan-Meier survival plot for zebrafish treated with various concentration of CDs (n=20). (b) and (c) Fluorescence microscopy images of

zebrafish larvae after incubating with CDs (3 mg/mL) for 24 h (c is an enlarged view of the intestine). (d) Fluorescence microscopy images after zebrafish larvae incubated with CDs 24h to transferred to E3 embryo media for another 24 h. (e) Average fluorescence intensity of zebrafish incubated for 24 hours with different concentrations of CDs (0 hours), and after 24 hours of incubation in CD-free media (24 hours).

To determine whether the CDs are biocompatible *in vivo*, we analyzed long-term survivability of zebrafish at different CDs concentrations (**Fig. 5a**). Zebrafish survival time was still normal with CD concentrations as high as 5 mg/mL, although a dose response was observed. When the concentration rose to 7 mg/mL, survival significantly decreased. The median survival time is shown in **Table S3.** The median survival time refers to the survival time corresponding to a survival rate of 50%. The median survival time, time at which 50% of the fish in a treatment are dead [63], of the zebrafish incubated with CDs at concentrations of the control, 0.5, 1, 3, 5, and 7 mg/mL was 11, 9, 8, 7.5, and 7 days, and 12 hours, respectively (**Table S3**). The results demonstrate that the CDs have very low toxicity even when concentrations reach as high as 5mg/mL, which is higher than the reported protective (from reactive oxygen species) concentration of nitrogen-doped CDs in zebrafish [41], and far higher than the imaging dose used in this study.

To illustrate the potential applications of CDs *in vivo*, we used fluorescent imaging to monitor the uptake, distribution, and metabolism of CDs in the transparent zebrafish (**Fig. 5b-e**). When the zebrafish were cultured for 24 h in E3 medium containing CDs, the bright blue and green fluorescence of the CDs was localized to the intestines and liver of the zebrafish (**Fig. 5b-c**). This adsorption pattern, adsorption from the intestines into the bloodstream and concentration in the liver, is consistent with reported results [64]. These zebrafish were then transferred to standard, CD-free, E3 medium and cultured for an additional 24 hours. The blue/green fluorescence was completely lost from the intestines and liver (**Fig. 5d**), demonstrating that they are readily excreted and do not bioaccumulate (**Fig. 5e**).

According to the requirements of US Food and Drug Administration (FDA), theranostic agents should be completely cleared from the body within a reasonable

period; this 24-hour clearance is within the norms of the field. Due to their low toxicity, easy, uptake, and easy clearance, CDs are good candidates for *in vivo* applications such as real-time multicolor bioimaging, molecular tracking, and potentially for theranostic drug delivery applications. Consequently, although cobalt toxicity or deficiency is not a major concern, we investigated whether the specific "Off-On" fluorescence sensing system with Co^{2+} and EDTA is compatible and possible in the zebrafish. The same fluorescence behaviour was observed in the animal as in the cell culture, indicating the as-prepared CDs sensor can be effect *in vivo* and *in vitro* (**Fig. 6**).

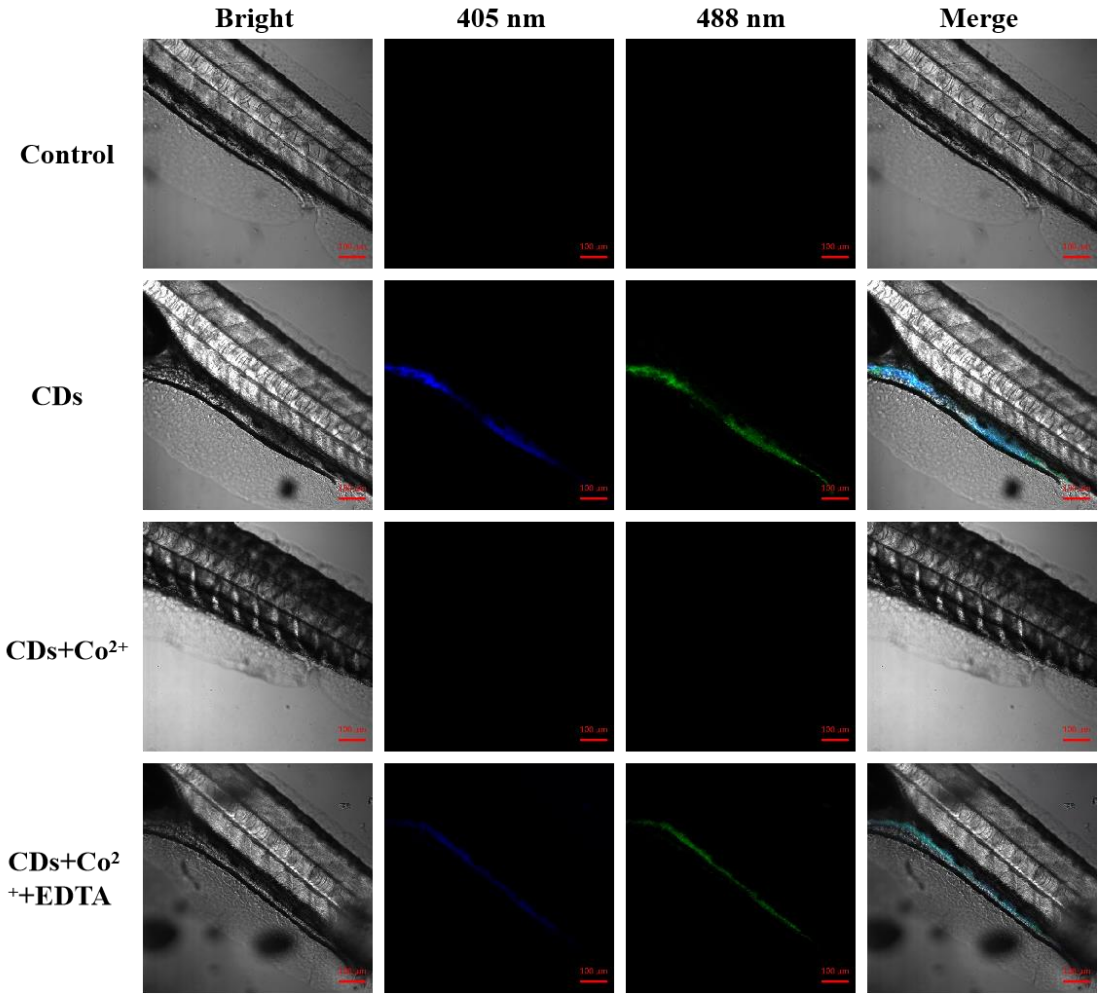

Fig. 6 Laser confocal microscopy images of zebrafish larvae incubated with CDs (3 mg/mL) for 24 h, and then treated with Co^{2+} (2 mM) and EDTA (8 mM) for 6 h before imaging under 405 nm and 488 nm excitation, respectively.

In view of the biocompatibility and efflux function of the prepared CDs, the as-prepared CDs will be loaded with drugs to explore their diagnostic and therapeutic potential. For instance, they can be used as potential drug carriers for the treatment of diseases such as Alzheimer's disease (AD) [64-66], and this will be reported on in due course as part of our ongoing collaboration.

3.5. Hiding and revealing information using CDs

An aqueous solution of CDs can also be used as a hidden fluorescent ink. Patterns were drawn onto filter paper, and air-dried (**Fig. 7**). The pattern could be clearly seen under 365 nm UV light as a bright blue symbol. When treated with Co^{2+}, the blue fluorescence was largely quenched, although not completely like in our recent report [67]. When the filter paper is retreated with an EDTA solution, the blue fluorescent outline is restored, allowing the hidden information to be retrieved. These CDs could have a role in product authentication.

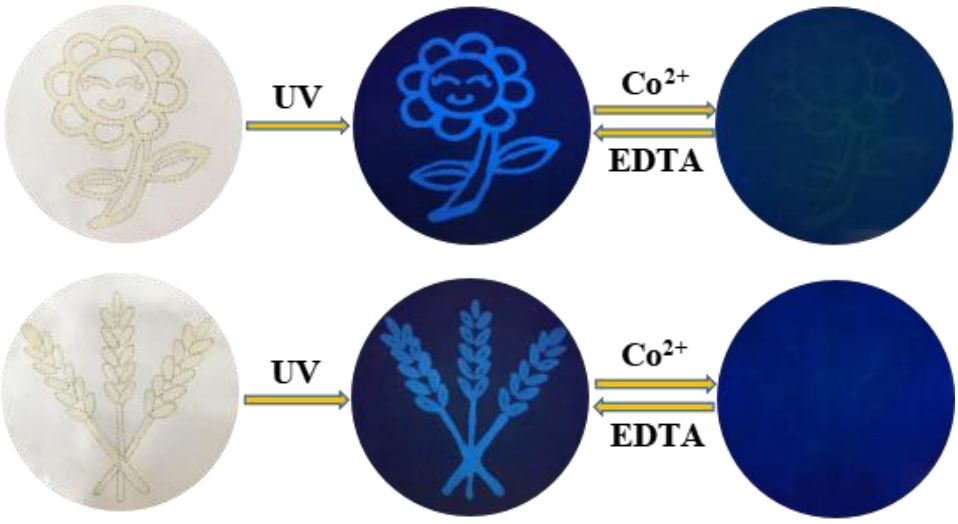

Fig. 7 Photographs of the fluorescent patterns on filter paper under bright light and UV light of patterns established using a CD ink, and then upon addition of Co^{2+} and EDTA solutions.

4. Conclusions

Using frozen tofu as a carbon source and ethylenediamine and phosphoric acid as nitrogen and phosphorus sources, we produced bright blue fluorescent, 2.9 nm diameter CDs in a high yielding (64%) hydrothermal synthesis. The fluorescence is

insensitive to metal ions with the exception of Co^{2+}, and as this ion can be stripped from the surface using a strong chelator like EDTA, these CDs act as very sensitive "off-on" fluorescence sensors for Co^{2+} and EDTA; detection limits were 58 nM and 98 nM, respectively. In addition, the aqueous solution of CDs can be used as fluorescent ink for information hiding and retrieval. The CDs are highly stable under a broad range of chemical conditions, and show low toxicity and rapid clearance, making them potentially useful for *in vivo* applications. These novel CDs could prove useful for drug delivery and theranostic applications, and studies are currently underway in this direction.

Conflicts of interest

There are no conflicts to declare.

CRediT Statement

Xiangping Wen: Methodology, Investigation, Resources, Data curation, Writing-original draft. **Guangming Wen:** Conceptualization, Methodology, Writing—review and editing. **Wenyan Li:** Investigation, Writing—review and editing. **Zhonghua Zhao:** Investigation, Writing—review and editing. **Xine Duan:** Investigation, Writing—review and editing. **Wenjun Yan:** Investigation, Writing—review and editing. **John F. Trant:** Methodology, Writing—Original Draft, Writing—review and editing, Funding Acquisition. **Yingqi Li:** Conceptualization, Methodology, Project Administration, Supervision, Writing—Original Draft, Writing—review and editing, Funding Acquisition.

Acknowledgements

This work was financially supported by the National Natural Science Foundation of China (Grant No. 21071091, 21671125, 21575083), the central government guiding local science and technology development special fund projects

(YDZX20191400002477), the Shanxi key research and development program (Social Development, Grant No. 201903D321105), the Shanxi Province “1331 project” key innovation team construction plan cultivation team (2018-CT-1), the China Scholarship Fund, the Transformation of Scientific and Technological Achievements Programs of Higher Education Institutions in Shanxi (2019KJ008), the Jinzhong College Innovation Team (jzxycxtd2019007), and the Natural Science and Engineering Research Council of Canada (2018-06338 to JFT).

References

[1] S.Y. Lim, W. Shen, Z. Gao, Carbon quantum dots and their applications, Chem. Soc. Rev. 44(1) (2015) 362-381.
[2] F. Wu, H. Su, X. Zhu, K. Wang, Z. Zhang, W.-K. Wong, Near-infrared emissive lanthanide hybridized carbon quantum dots for bioimaging applications, J. Mater. Chem. B 4(38) (2016) 6366-6372.
[3] J. Du, N. Xu, J. Fan, W. Sun, X. Peng, Carbon dots for *in vivo* bioimaging and theranostics, Small 15(32) (2019) 1805087.
[4] F. Wu, H. Su, K. Wang, W.K. Wong, X. Zhu, Facile synthesis of N-rich carbon quantum dots from porphyrins as efficient probes for bioimaging and biosensing in living cells, Int. J. Nanomed. 12 (2017) 7375-7391.
[5] M. Shamsipur, A. Barati, S. Karami, Long-wavelength, multicolor, and white-light emitting carbon-based dots: Achievements made, challenges remaining, and applications, Carbon 124 (2017) 429-472.
[6] Z. Yao, Z. Lai, C. Chen, S. Xiao, P. Yang, Full-color emissive carbon-dots targeting cell walls of onion for in situ imaging of heavy metal pollution, Analyst 144(11) (2019) 3685-3690.
[7] Y. Jiao, Y. Gao, Y. Meng, W. Lu, Y. Liu, H. Han, S. Shuang, L. Li, C. Dong, One-step synthesis of label-free ratiometric fluorescence carbon dots for the detection of silver ions and glutathione and cellular imaging applications, ACS Appl. Mater. Interfaces 11(18) (2019) 16822-16829.
[8] G.A.M. Hutton, B.C.M. Martindale, E. Reisner, Carbon dots as photosensitisers for solar-driven catalysis, Chem. Soc. Rev. 46(20) (2017) 6111-6123.
[9] H. Su, Y. Liao, F. Wu, X. Sun, H. Liu, K. Wang, X. Zhu, Cetuximab-conjugated iodine doped carbon dots as a dual fluorescent/CT probe for targeted imaging of lung cancer cells, Colloids Surf., B 170 (2018) 194-200.
[10] X. Miao, D. Qu, D. Yang, B. Nie, Y. Zhao, H. Fan, Z. Sun, Synthesis of carbon dots with multiple color emission by controlled graphitization and surface functionalization, Adv. Mater. (Weinheim, Ger.) 30(1) (2018) 1704740.
[11] S. Lu, R. Cong, S. Zhu, X. Zhao, J. Liu, J. S.Tse, S. Meng, B. Yang, pH-Dependent synthesis of novel structure-controllable polymer-carbon nanodots with high acidophilic luminescence and super carbon dots assembly for white

light-emitting diodes, ACS Appl. Mater. Interfaces 8(6) (2016) 4062-4068.
[12] L. Yue, H. Li, Q. Sun, J. Zhang, X. Luo, F. Wu, X. Zhu, Red-emissive ruthenium-containing carbon dots for bioimaging and photodynamic cancer therapy, ACS Appl. Nano Mater. 3(1) (2020) 869-876.
[13] X. Han, Z. Jing, W. Wu, B. Zou, Z. Peng, P. Ren, A. Wikramanayake, Z. Lu, R.M. Leblanc, Biocompatible and blood–brain barrier permeable carbon dots for inhibition of Aβ fibrillation and toxicity, and BACE1 activity, Nanoscale 9(35) (2017) 12862-12866.
[14] P.R. Sahoo, K. Prakash, S. Kumar, Synthesis of an oxadiazole through an indole mediated single step procedure for selective optical recognition of Cu^{2+} ions, Sens. Actuators, B 242 (2017) 299-304.
[15] J. Zuo, T. Jiang, X. Zhao, X. Xiong, S. Xiao, Z. Zhu, Preparation and application of fluorescent carbon dots, J. Nanomater. 2015 (2015) 787862.
[16] R. Sharma, K.V. Ragavan, M.S. Thakur, K.S.M.S. Raghavarao, Recent advances in nanoparticle based aptasensors for food contaminants, Biosens. Bioelectron. 74 (2015) 612-627.
[17] Y.-W. Zeng, D.-K. Ma, W. Wang, J.-J. Chen, L. Zhou, Y.-Z. Zheng, K. Yu, S.-M. Huang, N, S co-doped carbon dots with orange luminescence synthesized through polymerization and carbonization reaction of amino acids, Appl. Surf. Sci. 342 (2015) 136-143.
[18] G. Xu, Y. Niu, X. Yang, Z. Jin, Y. Wang, Y. Xu, H. Niu, Preparation of $Ti_3C_2T_x$ MXene-derived quantum dots with white/blue-emitting photoluminescence and electrochemiluminescence, Adv. Opt. Mater. 6(24) (2018) 1800951.
[19] M.R. Awual, M. Ismael, T. Yaita, Efficient detection and extraction of cobalt(II) from lithium ion batteries and wastewater by novel composite adsorbent, Sens. Actuators, B 191 (2014) 9-18.
[20] A.-I. Stoica, M. Peltea, G.-E. Baiulescu, M. Ionica, Determination of cobalt in pharmaceutical products, J. Pharm. Biomed. Anal. 36(3) (2004) 653-656.
[21] F. Barras, M. Fontecave, Cobalt stress in *Escherichia coli* and *Salmonella enterica*: Molecular bases for toxicity and resistance, Metallomics 3(11) (2011) 1130-1134.
[22] K. Sakthithasan, P. Lévy, J. Poupon, R. Garnier, A comparative study of edetate calcium disodium and dimercaptosuccinic acid in the treatment of lead poisoning in adults, Clin. Toxicol. 56(11) (2018) 1143-1149.
[23] T. Born, C.N. Kontoghiorghe, A. Spyrou, A. Kolnagou, G.J. Kontoghiorghes, EDTA chelation reappraisal following new clinical trials and regular use in millions of patients: review of preliminary findings and risk/benefit assessment, Toxicol. Mech. Methods 23(1) (2013) 11-17.
[24] C.A. McKay, Editorial: Use and misuse of metal chelation therapy, J. Med. Toxicol. 9(4) (2013) 301-302.
[25] M. Bhushan, M.H. Beck, Allergic contact dermatitis from disodium ethylenediamine tetra-acetic acid (EDTA) in a local anaesthetic, Contact Dermatitis 38(3) (1998) 183-183.
[26] M. Kimura, A. Kawada, Contact dermatitis due to trisodium

ethylenediaminetetra-acetic acid (EDTA) in a cosmetic lotion, Contact Dermatitis 41(6) (1999) 341-341.
[27] C.L. Sharratt, C.J. Gilbert, M.C. Cornes, C. Ford, R. Gama, EDTA sample contamination is common and often undetected, putting patients at unnecessary risk of harm, Int. J. Clin. Pract. 63(8) (2009) 1259-1262.
[28] S. Liao, F. Zhu, X. Zhao, H. Yang, X. Chen, A reusable P, N-doped carbon quantum dot fluorescent sensor for cobalt ion, Sens. Actuators, B 260 (2018) 156-164.
[29] J. Shi, C. Lu, D. Yan, L. Ma, High selectivity sensing of cobalt in HepG2 cells based on necklace model microenvironment-modulated carbon dot-improved chemiluminescence in Fenton-like system, Biosens. Bioelectron. 45 (2013) 58-64.
[30] K.R. Williams, V.Y. Young, B.J. Killian, Coulometric titration of ethylenediaminetetraacetate (EDTA) with spectrophotometric endpoint detection: An experiment for the instrumental analysis laboratory, J. Chem. Ed. 88(3) (2011) 315-316.
[31] D. Bano, V. Kumar, S. Chandra, V.K. Singh, S. Mohan, D.K. Singh, M. Talat, S.H. Hasan, Synthesis of highly fluorescent nitrogen-rich carbon quantum dots and their application for the turn-off detection of cobalt (II), Opt. Mater. 92 (2019) 311-318.
[32] N. Jing, M. Tian, Y. Wang, Y. Zhang, Nitrogen-doped carbon dots synthesized from acrylic acid and ethylenediamine for simple and selective determination of cobalt ions in aqueous media, J. Lumin. 206 (2019) 169-175.
[33] B. Narola, A.S. Singh, M. Mitra, P.R. Santhakumar, T.G. Chandrashekhar, A validated reverse phase HPLC method for the determination of disodium EDTA in meropenem drug substance with UV-detection using precolumn derivatization technique, Anal. Chem. Insights 6 (2011) 7-14.
[34] A.A. Krokidis, N.C. Megoulas, M.A. Koupparis, EDTA determination in pharmaceutical formulations and canned foods based on ion chromatography with suppressed conductimetric detection, Anal. Chim. Acta 535(1) (2005) 57-63.
[35] C. Zhao, X. Li, C. Cheng, Y. Yang, Green and microwave-assisted synthesis of carbon dots and application for visual detection of cobalt(II) ions and pH sensing, Microchem. J. 147 (2019) 183-190.
[36] T. Hallaj, M. Amjadi, J.L. Manzoori, R. Shokri, Chemiluminescence reaction of glucose-derived graphene quantum dots with hypochlorite, and its application to the determination of free chlorine, Microchim. Acta 182(3) (2015) 789-796.
[37] M. Yang, Q. Tang, Y. Meng, J. Liu, T. Feng, X. Zhao, S. Zhu, W. Yu, B. Yang, Reversible “off–on” fluorescence of Zn^{2+}-passivated carbon dots: Mechanism and potential for the detection of EDTA and Zn^{2+}, Langmuir 34(26) (2018) 7767-7775.
[38] R. Lowe, E.P. Go, G.C. Tong, N.H. Voelcker, G. Siuzdak, Monitoring EDTA and endogenous metabolite biomarkers from serum with mass spectrometry, Spectroscopy 19 (2005) 137-146.
[39] H. Chen, F. Yuan, J. Xu, Y. Zhang, Y. Wu, L. Wang, Simple and sensitive detection method for Cobalt(II) in water using $CePO_4:Tb^{3+}$ nanocrystals as fluorescent probes, Spectrochim. Acta, Part A 107 (2013) 151-155.
[40] L. Zi, Y. Huang, Z. Yan, S. Liao, Thioglycolic acid-capped $CuInS_2$/ZnS quantum

dots as fluorescent probe for cobalt ion detection, J. Lumin. 148 (2014) 359-363.
[41] L. Wang, B. Li, L. Li, F. Xu, Z. Xu, D. Wei, Y. Feng, Y. Wang, D. Jia, Y. Zhou, Ultrahigh-yield synthesis of N-doped carbon nanodots that down-regulate ROS in zebrafish, J. Mater. Chem. B 5(38) (2017) 7848-7860.
[42] A.J. Hill, H. Teraoka, W. Heideman, R.E. Peterson, Zebrafish as a model vertebrate for investigating chemical toxicity, Toxicol. Sci. 86(1) (2005) 6-19.
[43] R.-M. Ferraiuolo, D. Meister, D. Leckie, M. Dashti, J. Franke, L.A. Porter, J.F. Trant, Neuro and heparic toxicological profile of (*S*)-2,4-diaminobutyric acid in embryonic, adolescent and adult zebrafish, J. Appl. Toxicol. 39 (2019) 1568-1577.
[44] X. Li, S. Zhang, S.A. Kulinich, Y. Liu, H. Zeng, Engineering surface states of carbon dots to achieve controllable luminescence for solid-luminescent composites and sensitive Be^{2+} detection, Sci. Rep. 4(1) (2014) 4976.
[45] S. Zhu, J. Zhang, S. Tang, C. Qiao, L. Wang, H. Wang, X. Liu, B. Li, Y. Li, W. Yu, X. Wang, H. Sun, B. Yang, Surface chemistry routes to modulate the photoluminescence of graphene quantum dots: From fluorescence mechanism to up-conversion bioimaging applications, Adv. Funct. Mater. 22(22) (2012) 4732-4740.
[46] K. Li, W. Liu, Y. Ni, D. Li, D. Lin, Z. Su, G. Wei, Technical synthesis and biomedical applications of graphene quantum dots, J. Mater. Chem. B 5(25) (2017) 4811-4826.
[47] H. Peng, J. Travas-Sejdic, Simple aqueous solution route to luminescent carbogenic dots from carbohydrates, Chem. Mater. 21(23) (2009) 5563-5565.
[48] Y. Yang, J. Cui, M. Zheng, C. Hu, S. Tan, Y. Xiao, Q. Yang, Y. Liu, One-step synthesis of amino-functionalized fluorescent carbon nanoparticles by hydrothermal carbonization of chitosan, Chem. Commun. 48(3) (2012) 380-382.
[49] R. Liu, D. Wu, S. Liu, K. Koynov, W. Knoll, Q. Li, An aqueous route to multicolor photoluminescent carbon dots using silica spheres as carriers, Angew. Chem. Int. Ed. 48(25) (2009) 4598-4601.
[50] H. Li, Z. Kang, Y. Liu, S.-T. Lee, Carbon nanodots: Synthesis, properties and applications, J. Mater. Chem. 22(46) (2012) 24230-24253.
[51] F. Zu, F. Yan, Z. Bai, J. Xu, Y. Wang, Y. Huang, X. Zhou, The quenching of the fluorescence of carbon dots: A review on mechanisms and applications, Microchim. Acta 184(7) (2017) 1899-1914.
[52] Z. Bai, F. Yan, J. Xu, J. Zhang, J. Wei, Y. Luo, L. Chen, Dual-channel fluorescence detection of mercuric (II) and glutathione by down- and up-conversion fluorescence carbon dots, Spectrochim. Acta, Part A 205 (2018) 29-39.
[53] X. Wen, Z. Zhao, S. Zhai, X. Wang, Y. Li, Stable nitrogen and sulfur co-doped carbon dots for selective folate sensing, *in vivo* imaging and drug delivery, Diamond Relat. Mater. 105 (2020) 107791.
[54] D. Lebeau, P.E. Reiller, C. Lamouroux, Direct analysis of ethylenediaminetetraacetic acid (EDTA) on concrete by reactive-desorption electrospray ionization mass spectrometry, Talanta 132 (2015) 877-883.
[55] U. Holtkamp, J. Klein, J. Sander, M. Peter, N. Janzen, U. Steuerwald, O. Blankenstein, EDTA in dried blood spots leads to false results in neonatal endocrinologic screening, Clin. Chem. 54(3) (2008) 602-605.

[56] L. Li, L. Tian, Y. Wang, W. Zhao, F. Cheng, Y. Li, B. Yang, Smart pH-responsive and high doxorubicin loading nanodiamond for in vivo selective targeting, imaging, and enhancement of anticancer therapy, J. Mater. Chem. B 4(29) (2016) 5046-5058.
[57] F. Du, Z. Cheng, M. Kremer, Y. Liu, X. Wang, S. Shuang, C. Dong, A label-free multifunctional nanosensor based on N-doped carbon nanodots for vitamin B_{12} and Co^{2+} detection, and bioimaging in living cells and zebrafish, J. Mater. Chem. B 8(23) (2020) 5089-5095.
[58] C.-L. Li, C.-C. Huang, A.P. Periasamy, P. Roy, W.-C. Wu, C.-L. Hsu, H.-T. Chang, Synthesis of photoluminescent carbon dots for the detection of cobalt ions, RSC Adv. 5(3) (2015) 2285-2291.
[59] S.Y. Chae, H.J. Kim, M.S. Lee, Y.L. Jang, Y. Lee, S.H. Lee, K. Lee, S.H. Kim, H.T. Kim, S.-C. Chi, T.G. Park, J.H. Jeong, Energy-independent intracellular gene delivery mediated by polymeric biomimetics of cell-penetrating peptides, Macromol. Biosci. 11(9) (2011) 1169-1174.
[60] T.-G. Iversen, T. Skotland, K. Sandvig, Endocytosis and intracellular transport of nanoparticles: Present knowledge and need for future studies, Nano Today 6(2) (2011) 176-185.
[61] L. Li, L. Tian, W. Zhao, Y. Li, B. Yang, Acetate ions enhance load and stability of doxorubicin onto PEGylated nanodiamond for selective tumor intracellular controlled release and therapy, Integr. Biol. 8(9) (2016) 956-967.
[62] Y. Li, Y. Tong, R. Cao, Z. Tian, B. Yang, P. Yang, *In vivo* enhancement of anticancer therapy using bare or chemotherapeutic drug-bearing nanodiamond particles, Int. J. Nanomed. 9 (2014) 1065-82.
[63] Q.-Q. Shi, Y.-H. Li, Y. Xu, Y. Wang, X.-B. Yin, X.-W. He, Y.-K. Zhang, High-yield and high-solubility nitrogen-doped carbon dots: formation, fluorescence mechanism and imaging application, RSC Adv. 4(4) (2014) 1563-1566.
[64] I. Javed, Z. Zhang, J. Adamcik, N. Andrikopoulos, Y. Li, D.E. Otzen, S. Lin, R. Mezzenga, T.P. Davis, F. Ding, P.C. Ke, Accelerated amyloid beta pathogenesis by bacterial amyloid FapC, Adv. Sci. 7(18) (2020) 2001299.
[65] I. Javed, G. Peng, Y. Xing, T. Yu, M. Zhao, A. Kakinen, A. Faridi, C.L. Parish, F. Ding, T.P. Davis, P.C. Ke, S. Lin, Inhibition of amyloid beta toxicity in zebrafish with a chaperone-gold nanoparticle dual strategy, Nat. Commun. 10(1) (2019) 3780.
[66] F. Xin, Y. Li, C. Fu, I. Javed, X. Huang, A. Schaschkow, R.S. Garcia Ribeiro, E.N. Gurzov, T.P. Davis, X. Zhang, P.C. Ke, R. Qiao, Multimodal nanoprobe for pancreatic beta cell detection and amyloidosis mitigation, Chem. Mater. 32(3) (2020) 1080-1088.
[67] W. Li, X. Wen, H. Zhao, W. Yan, J.F. Trant, Y. Li, Acid-triggered self-assembled egg white protein-coated gold nanoclusters for selective fluorescent detection of Fe^{3+}, NO^{2-}, and Cysteine, ACS Appl. Nano Mater. 3(12) (2020) 11838-11849.